Energy efficiency improvement of Gijang SWRO plant in Busan, Korea

Yeonghyeok Kim, Seungwon Ihm*, Sungwoo Woo

*Doosan Heavy Industries & Construction, 465 Gangnam-daero, Seocho-Gu, Seoul 06611, Korea, Tel. +82 2 513 7274;
Fax: +82 2 513 6217; email: seungwon.ihm@doosan.com (S. Ihm), Tel. +82 2 513 7273; Fax: +82 2 513 6217;
email: yeonghyeok.kim@doosan.com (Y. Kim), Tel. +82 2 513 6184; Fax: +82 2 513 6217;
email: sungwoo.woo@doosan.com (S. Woo)*

ABSTRACT

For seawater reverse osmosis (SWRO), the electrical energy consumption by pumps takes a major share in the water production cost, thus the optimal design and operation of the major process pumps are essential. Two major pumps in SWRO are the seawater supply pump (SSP) and the high pressure pump (HPP). In order to improve the energy efficiency of the 2 million imperial gallons per day (MIGD) line of the Gijang SWRO plant in Busan, Korea, the required hydraulic head of the SSP is analyzed from the plant operation data and the SSP head is adjusted by removing one of the four impeller stages and trimming the remaining impellers. In addition, a variable frequency drive is added to the existing HPP for optimal operation to the seasonal seawater temperature variation. The energy savings are carefully evaluated from the plant operation data, and it is found that about 89 kW from the SSP and 105–326 kW from the HPP could be saved. In terms of specific power consumption (SPC), these are 0.221 and 0.261–0.811 kWh/ton reduction. Second law (exergetic) analyses are conducted and it is found that the unnecessary exergy destructions in the pressure regulating valve after the SSP and the control valve after the HPP are minimized from the modifications. The second law efficiency of the Gijang 2 MIGD line is improved from 42.83% to 46.61%, resulting in the SPC drop from 4.213 to 3.493 kWh/ton at about 16°C based on the first pass SWRO permeate water flow rate.

Keywords: Gijang seawater reverse osmosis (SWRO) plant; Energy efficiency; Exergy analysis; Second law efficiency; Seawater supply pump (SSP); High pressure pump (HPP); Variable frequency driver (VFD)

1. Introduction

Because of population and economic growth and climate change, water shortage has become a serious issue worldwide. Korea is not an exception of the countries experiencing water shortage – droughts are more frequent for Korea [1,2], causing a heavy impact on farmers and local drinking water shortages. As a measure to secure fresh water resources, the construction of the first seawater desalination plant in Korea, Gijang seawater reverse osmosis (SWRO) plant, started in 2010 [3,4] and the plant was successfully commissioned in 2014 [5]. In order to promote seawater desalination as a more useful alternative water resource, the cost of product water

from desalination should be sufficiently low to municipal and industrial demands. Seawater desalination is an energy intensive technology and the energy cost takes a major share in the desalinated water production cost [6,7], thus the reduction of electrical energy consumption of SWRO plant is the key to produce fresh water from seawater economically.

The total water production capacity of Gijang SWRO is 10 MIGD (1 million imperial gallons per day = 45,460 m³/d), and there are 8 and 2 MIGD lines. As per the Korean government R&D program, improving energy efficiency of the 2 MIGD line, which is a dissolved air flotation with ball filter (DABF) – ultrafiltration (UF) – reverse osmosis (RO) system, has been studied. For a full SWRO system, it is well known that the primary electricity consumption is for the "RO" part

* Corresponding author.

and the second is for the "intake" [8]. This is true for the Gijang 2 MIGD line as well, high pressure pump (HPP) and seawater supply pump (SSP) are of the two largest energy consumption parts. Therefore, improving energy efficiency of the two major pumps is the key to improve the overall SWRO efficiency. Two possible approaches are considered here. The first is the optimization of a pump design margin while securing a stable operating point in terms of flow rate and pressure from the operation data. Practically, pump impeller redesign could be considered [9,10]. The second approach is the introduction of a variable frequency drive (VFD) [11,12]. This is especially important and viable for HPP, because the required feed pressure for SWRO membranes varies depending on seawater temperature, which is 10°C for winter and 25°C for summer design condition at Gijang.

In order to evaluate the performance improvement from the modification works, exergy analysis is considered in addition to a typical power consumption comparison. Exergy analysis has been a popular tool to analyze the desalination system in terms of an overall process as well as a component-wise energy efficiency evaluation. Hamed et al. [13] analyzed (plane) multi-effect distillation (MED), MED with thermo vapor compressor (MED-TVC) and MED with mechanical vapor compressor (MED-MVC) for several top brine temperatures and the numbers of effects in an evaporator design, and found out that MED-TVC was the most efficient system in terms of second law efficiency among the analyzed MEDs, and that the most exergy destruction occurred at the first effect and TVC while the destruction significantly reduced with more number of effects and improved TVC performance. Mistry et al. [14] analyzed different desalination technologies of MED, multi-stage flash, direct contact membrane distillation, MVC, SWRO and humidification–dehumidification, and compared the processes in terms

of second law efficiency. Component-wise contribution of entropy generation in each desalination system revealed which component needed to be improved for a better system efficiency. More recently, Blanco-Marigorta et al. [15] applied the exergetic efficiency analysis as a performance evaluation tool in SWRO plants in operation. Thanks to the special feature of the 10 parallel SWRO lines with different pumps, pretreatments, energy recovery devices, and so on, with the same seawater pond at the same site, the component by component exergetic efficiencies could be compared, and finally some components performing better and some other components requiring maintenance or replacement were specified.

In this paper, the analysis and optimization of SSP and HPP in the Gijang 2 MIGD line is introduced. The details of pump modifications are explained and the electrical energy saving is shown with the actual operation data. Second law (exergy) analysis is conducted to understand the energy structure of the Gijang SWRO desalination plant. The quantitative exergetic data before and after the modifications provide an important insight to designers – in which component the most exergetic loss may exist and how much the overall plant efficiency could be improved.

2. Plant and site conditions

2.1. System configuration of Gijang 2 MIGD line

The Gijang SWRO desalination plant is located at the south-east end of Korean peninsula, in the city of Busan, Korea. With its design capacity of 10 MIGD (=45,460 m³/d), the plant is constructed on the skirt of a mountain. Fig. 1 shows the major processes and buildings in the bird's eye view of the Gijang SWRO plant. The special feature of its intake system, which is directly connected to the DABF through an underground
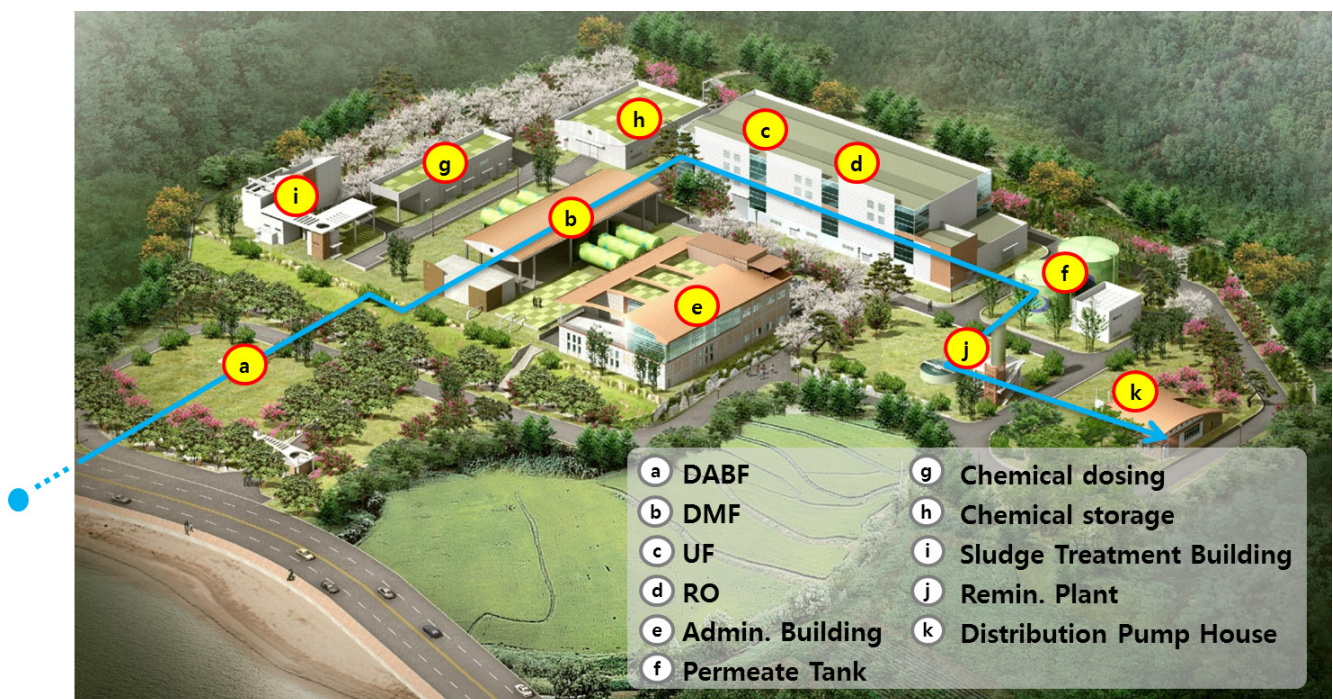

Fig. 1. Bird's eye view of the Gijang SWRO plant [3].

tunnel, is described in detail in a study by Woo et al. [3]. As shown in Fig. 2, Gijang SWRO consists of two lines with different pretreatment technologies. DABF – UF – SWRO with turbo charger (T/C) is for the 2 MIGD line, and DABF – dual media filter – SWRO with dual work exchange energy recovery is for the 8 MIGD line [4]. In this paper, the 2 MIGD line is of interest as per the Korean government R&D program.

The common intake is placed at 300 m off the beach, and there are passive offshore screen, intake pipe and air-burst cleaning system [3]. Intake pipe is directly connected to the DABF, which is installed under the ground level, thus seawater flows into the DABF by gravity. The DABF could be operated in three different modes as shown in Fig. 3 [4], depending on the raw seawater quality. Usually ball filter
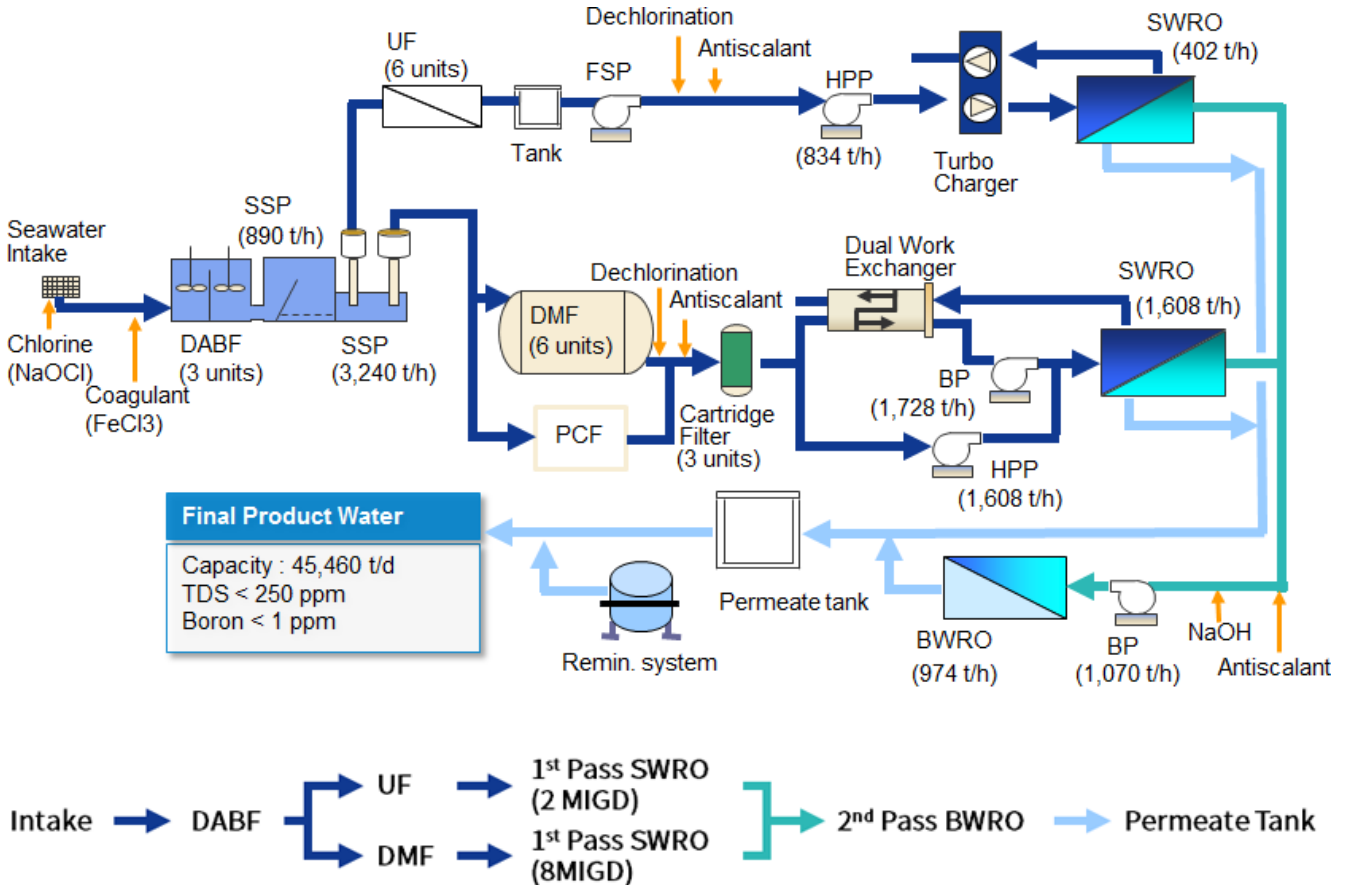

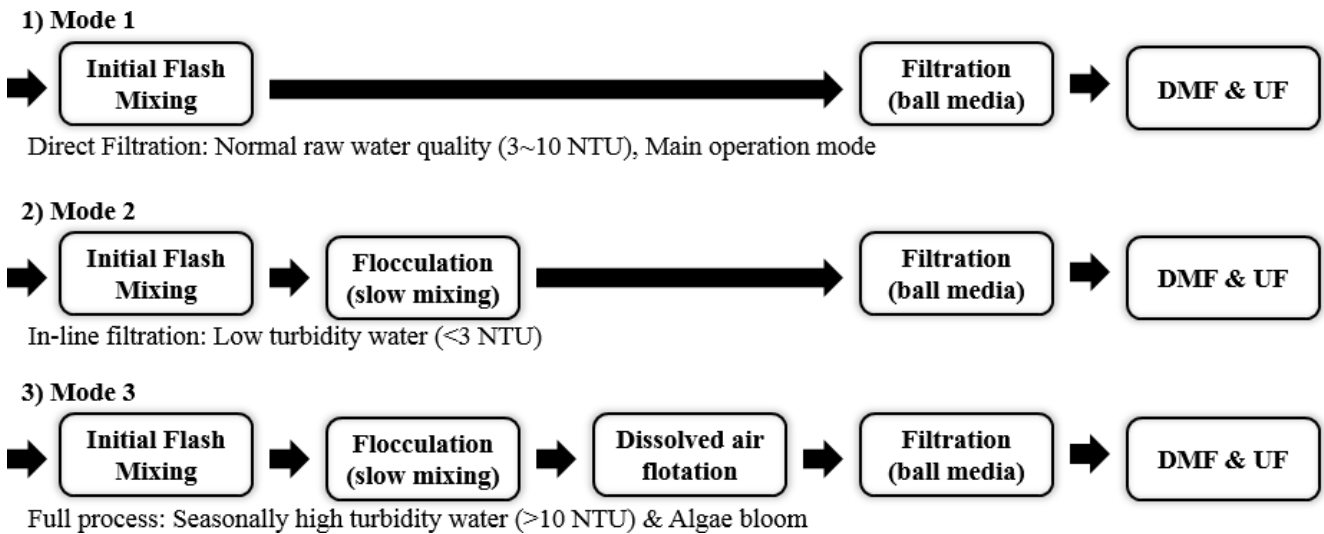Fig. 2. Process flow diagram of the Gijang SWRO plant [4].

Fig. 3. Schematics of various operation modes of the DABF system [4].

(mode 1 and 2) is operated while flotation turns on (mode 3) during high turbidity and/or algae bloom season.

The treated water from the DABF is supplied to the UF system by the SSP. The filtered water from the UF is supplied to the RO system through the filtered water supply pump (FSP). Finally the HPP and the T/C pressurize the feed water to produce the fresh water from the 16-inch RO membranes.

2.2. Seawater temperature and salinity

Fig. 4 shows the monthly averaged seawater temperature and salinity at Busan, Korea, in 2015. Standard deviations (σ) from daily average values are appeared as bars from the monthly averaged values indicating ±1σ. The seawater temperature was observed as 11.5°C in February and 23.5°C in August as monthly average, and the minimum and maximum daily averaged temperatures were observed as 10.7°C in February and 26.5°C in August, respectively. The monthly seawater salinity was varying from 31,800 mg/L in July–September to 34,000 mg/L in February–March, and the minimum and maximum daily averaged salinities were observed as 30,400 mg/L in July and 34,100 mg/L in January–March, respectively. It is clear that the seawater temperature and salinity are affected by the seasonal characteristics of Korea, that is, cold and drought weather in winter and hot and rainy weather in summer. Especially, the seasonal temperature difference triggers the need of optimal operation of the HPP in terms of energy consumption depending on the required feed pressure for the SWRO plant.

3. Pump modification

3.1. Seawater supply pump modification

The SSP serves to supply the DABF treated water to the UF system and maintain the required feed pressure for the UF membrane. The UF system periodically performs chemical enhanced backwash and clean in place. With the operation time accumulated, foreign substances that have not been removed by cleaning will be piled up and the membranes would be contaminated. Due to the degradation of the membrane, the permeability becomes smaller and more pressure is required to keep the flow rate. Therefore, the design pressure at the UF feed should have a certain amount of margin. The initial head of the SSP was designed as 67 m considering this margin. Through the development of a new UF product by the supplier, however, the specification of the UF membrane has been improved, which resulted in a less feed pressure requirement. In addition, there was a pressure regulating valve (PRV) before the UF to protect the UF membranes from unnecessary pressure peak. During the operation stage, it is found that the PRV has a surplus margin which needs to be optimized. Finally, it is concluded that 47 m instead of 67 m should be sufficient for the head of the SSP. It is well known that there are possible improvement methods for an oversized centrifugal pump, such as trimming the existing pump impeller, installing a smaller impeller, removing some stages of the pump (in case of a multi-stage pump), replacing with a smaller pump, or reducing the pump speed, and that lower maintenance cost and longer equipment life could be expected if the modified pump operates closer to its (new) best efficiency point [17].
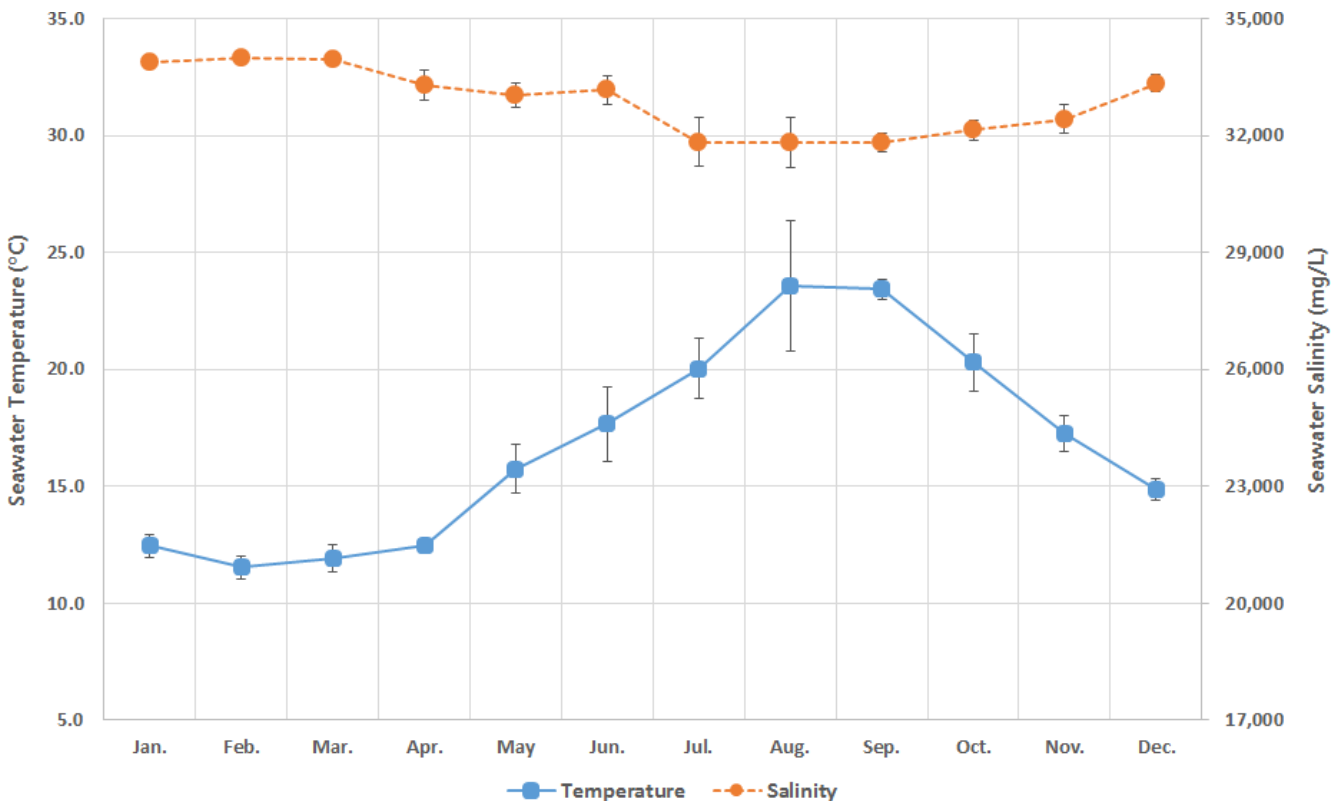

Fig. 4. Monthly seawater temperature and salinity at Busan, Korea in 2015 [16] (the bars indicate standard deviation (σ) of the month as per the daily average values: ±1σ).

In order to reduce the head of the SSP by 20 m, first the number of impeller stages is changed from its original 4th stage to the revised 3rd stage as shown in Fig. 5.

Besides, the remaining three impellers' outer diameter is trimmed to achieve the target pump head. It is well known that for a centrifugal pump, reducing the outside impeller diameter represents a relatively simple and hydraulically effective method to meet the practical requirements by changing the performance curves of pumps [9,10,17,18]. Fig. 6 illustrates the advantages of trimming impellers. It is clear that trimming impellers could save the electrical energy by minimizing the head loss at the following valves.
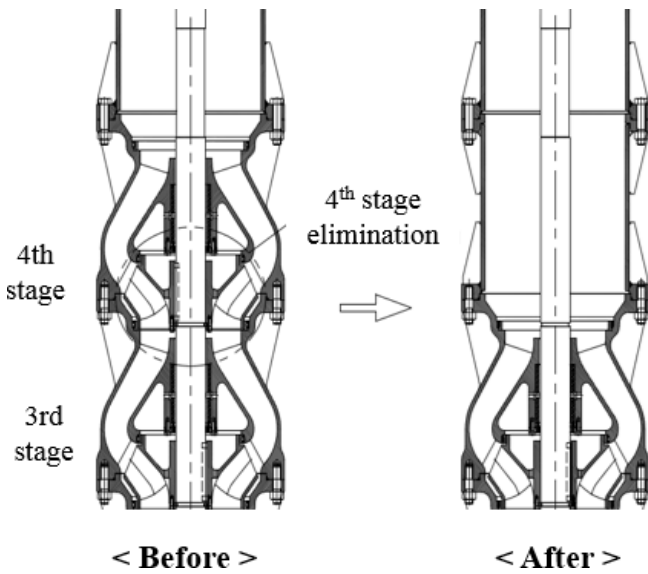
Moreover, if there is a room to the cross point between the system resistance curve and the pump performance curve in terms of flow rate, the trimmed impeller pump could have a higher maximum flow rate at the limit of the driver power.

Fig. 7 shows the actual performance and power consumption of the SSP before and after the modifications. The dots in Fig. 7 are the shop test results by the manufacturer after the modification. As indicated, the head of the modified SSP is decreased by about 20 m, compared with the original SSP head of 67 m at the same design flow rate of 890 m³/h, as marked with the red circles in Fig. 7. The shaft power of the original SSP increases with a flow rate increase, while that of the modified SSP shows a much gentler slope. Finally, the modified SSP is expected to save about 30% of its original power consumption at the design flow rate.

3.2. High pressure pump modification

The HPP capacity is 835 m³/h and the design head is 400 m. A control valve is installed at the discharge of the HPP, and the seawater from the control valve is further pressurized by the T/C and is supplied to the SWRO membrane. In the SWRO membrane, the incoming seawater is separated into fresh water (permeate) and concentrated brine (concentrate) which salinity is about 6.6%. The rejected brine still has a high pressure and flows into the turbine section of the T/C. Another turbine installed on the opposite side rotates and pressurizes the feed seawater to meet the required SWRO feed pressure. After the T/C, the brine is discharged from the system with lowered pressure.

Lower operating pressure at the feed of the SWRO membrane is required in the case of higher seawater temperatures and/or low levels of membrane aging and fouling. Originally, however, the HPP is designed to run at a constant impeller

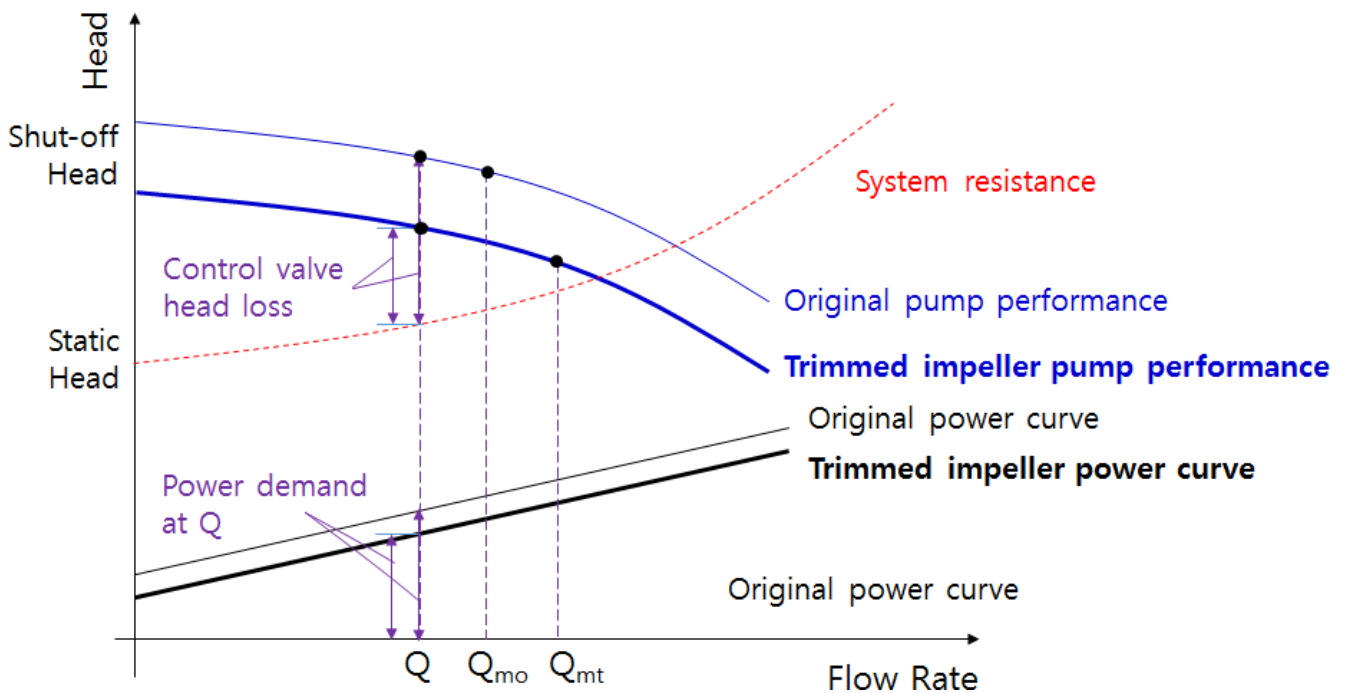Fig. 5. Modification of the seawater supply pump.

Fig. 6. Advantage of trimming impellers (selectively reproduced from a study by Shiels [9]) (Q_{mo} is the maximum flow rate at limit of driver power with original impeller and Q_{mt} is the maximum flow rate at limit of driver power with trimmed impeller).
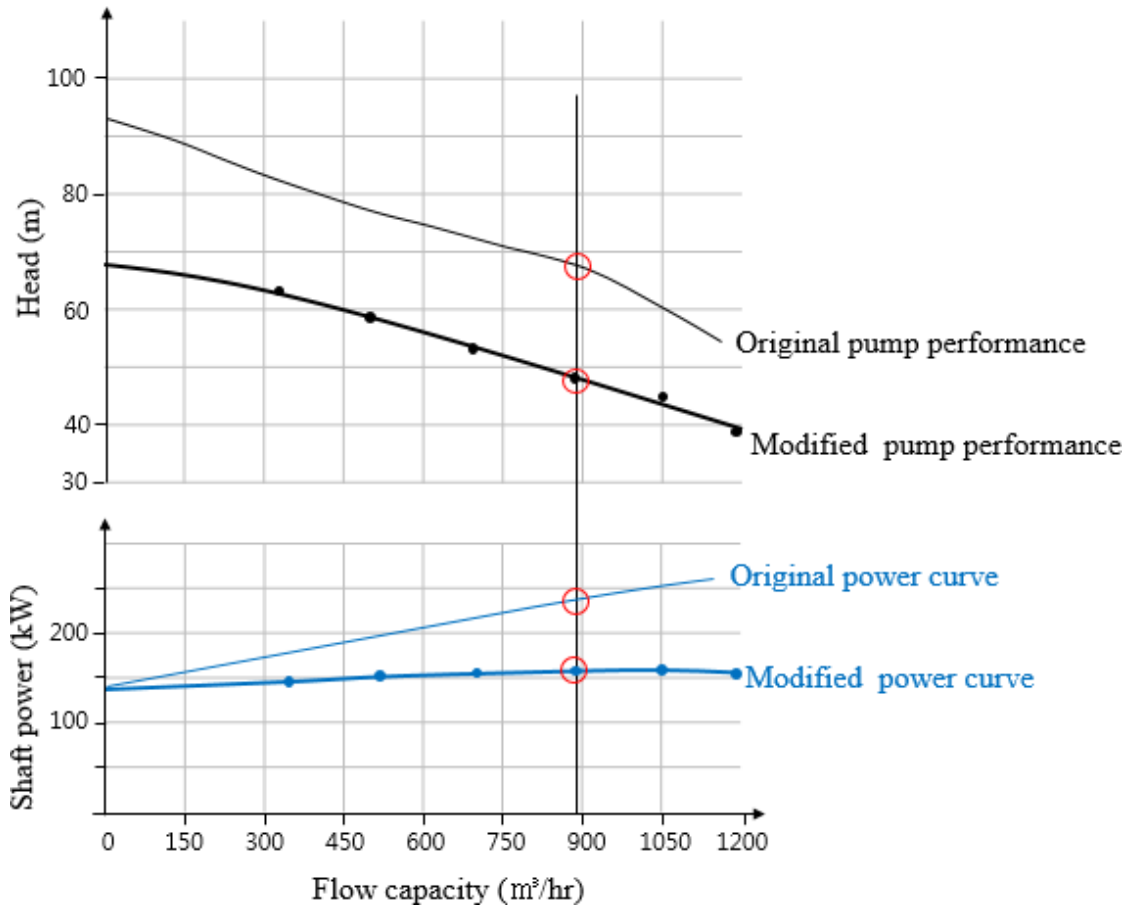
Fig. 7. Performance and power curves of the original and modified SSP for the Gijang 2 MIGD line.

rotation speed. In order to maintain the same fresh water production, a control valve is installed at the discharge of the HPP, adjusting the feed pressure at the SWRO membrane. Therefore, the pressure drop in this control valve is understood as the wasted power in the HPP-SWRO system. Technical and economic feasibilities are studied considering the seasonal seawater temperature change to compare a VFD installation cost and an expected electricity cost savings, then the installation of a VFD is decided. Fig. 8 shows the different performance diagrams for a typical constant speed pump and for a pump with a VFD. At the same flow rate, a pump with a VFD could generate different discharge pressures by varying the motor speed. The specifications of the high pressure pump, motor, and inverter (VFD) used for the Gijang 2 MIGD line can be found in Table 1. The new VFD was installed at the end of 2015 and the HPP started its operation with the VFD from 2016.

The performance curve of the HPP with VFD is illustrated in Fig. 9. At the design flow rate of 834 ton/h, R1 and R2 are the estimated discharge pressure range, in which the motor speed will vary from 83% to 100%.

4. Exergy analysis

4.1. Mathematical model

Second law (exergy) analysis is needed to place all energy interactions on the same basis and to give relevant guidance
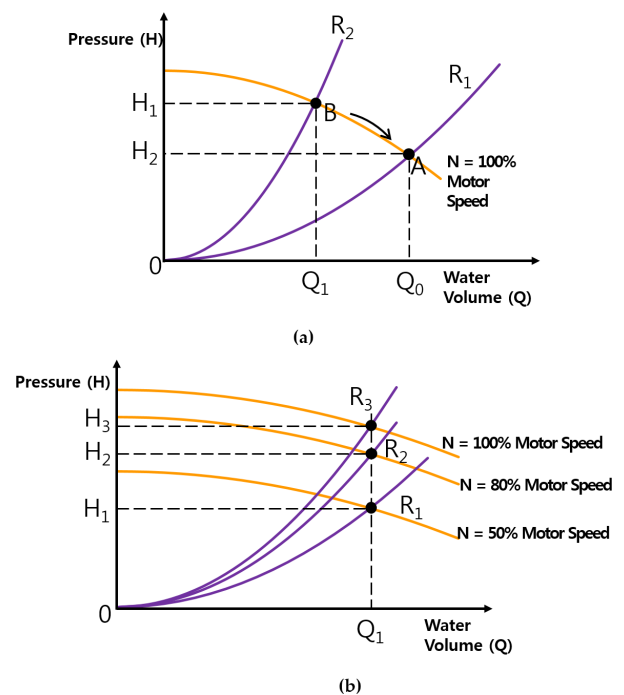

Fig. 8. Performance diagram for (a) constant speed pump and (b) variable speed pump.

Table 1
Specification of the HPP, motor and inverter (VFD)

Pump	Model	300 × 250 RN
	Type	Centrifugal pump
	Differential head	400 m
	Capacity	835 m³/h
	Efficiency	83%
	Minimum continuous flow	200 m³/h
Motor	Type	HRQ3 451-26E
	Power	1,350 kW
	RPM	3,570
	Volts/phase/cycles	6,600/3/60
	Full load AMPs	137.3A
	Efficiency	94.5% @100% load, 94.2% @75% load, 93.3% @50% load
	Power factor	91%
Inverter	Model	N5000-1700H6 IGBT
	Rated output	1,700 kW
	Phases	3
	Rated frequency	0–60 Hz
	Rated voltage	6.6 kV
	Rated current	175 A
	Efficiency	97%

for process improvement [13]. Especially, it has been a useful tool to understand a component-wise energy efficiency. For many exergy analyses for a RO system, only thermomechanical and chemical exergies are considered [19], because they are the two major exergy components while other exergy components include kinetic and potential [20,21]. The classification of exergy is shown in Fig. 10 [20].

Especially for the Gijang SWRO Plant, the potential component of exergy is very important to understand the overall process and component-wise efficiency, because the plant is located on the skirt of a mountain, thus the level difference is a must to consider. Fig. 11 shows the contour lines of the plant and a sectional view of pipeline from SSP toward pretreatment area is illustrated in Fig. 12 for better understanding.

Finally, the following equation for flow exergy is considered in this paper:

$$e_f = \frac{v^2}{2} + g\left(l - l^*\right) + \left(h - h^*\right) - T_0\left(s - s^*\right) + \sum_{i=1}^{n} y_i\left(\mu_i^* - \mu_i^0\right) \tag{1}$$

where v is the flow velocity, g is the gravitational acceleration (=9.81 m/s^2), l is the level and h, s, y and μ are the specific enthalpy, entropy, mass fraction and chemical potential, respectively.

In Eq. (1), the first term represents the kinetic exergy, the second is the potential and the third and the fourth are the thermomechanical and the last is the chemical exergy components. The thermomechanical and the chemical exergy functions are validated with the examples in a study by Sharqawy et al. [19], which are summarized in Appendix A.

In this paper, the exergetic efficiency of a component and/or a system is defined as follows:

$$\eta_{II} = \sum \dot{E}_{out} / \sum \dot{E}_{in} \tag{2}$$

where $\dot{E}$ is the exergy rate of not only for the incoming and outgoing "flow" streams but also for any other form of energy streams, for example, electricity. The subscript "in" and "out" indicates stream inward to and outgoing from the interested component and/or the system.
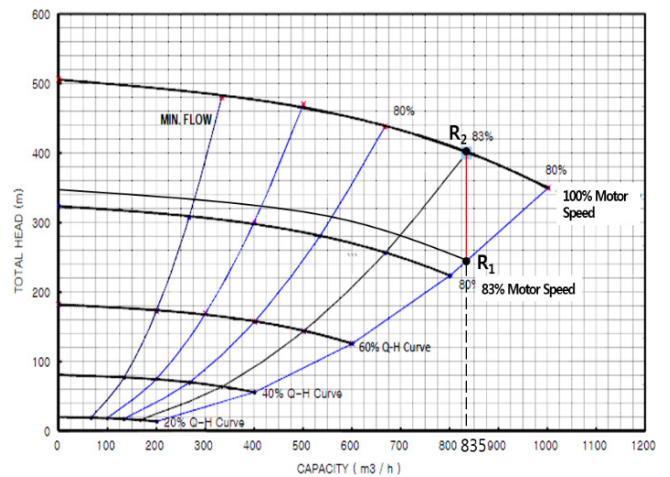
Fig. 9. Performance curve of the HPP with VFD.
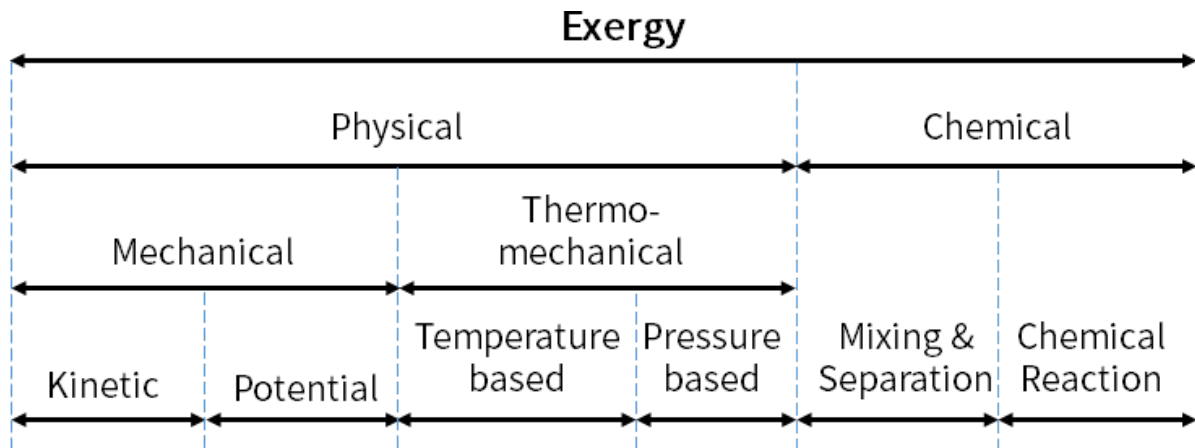
Fig. 10. Classification of exergy for P–V–T system [20].
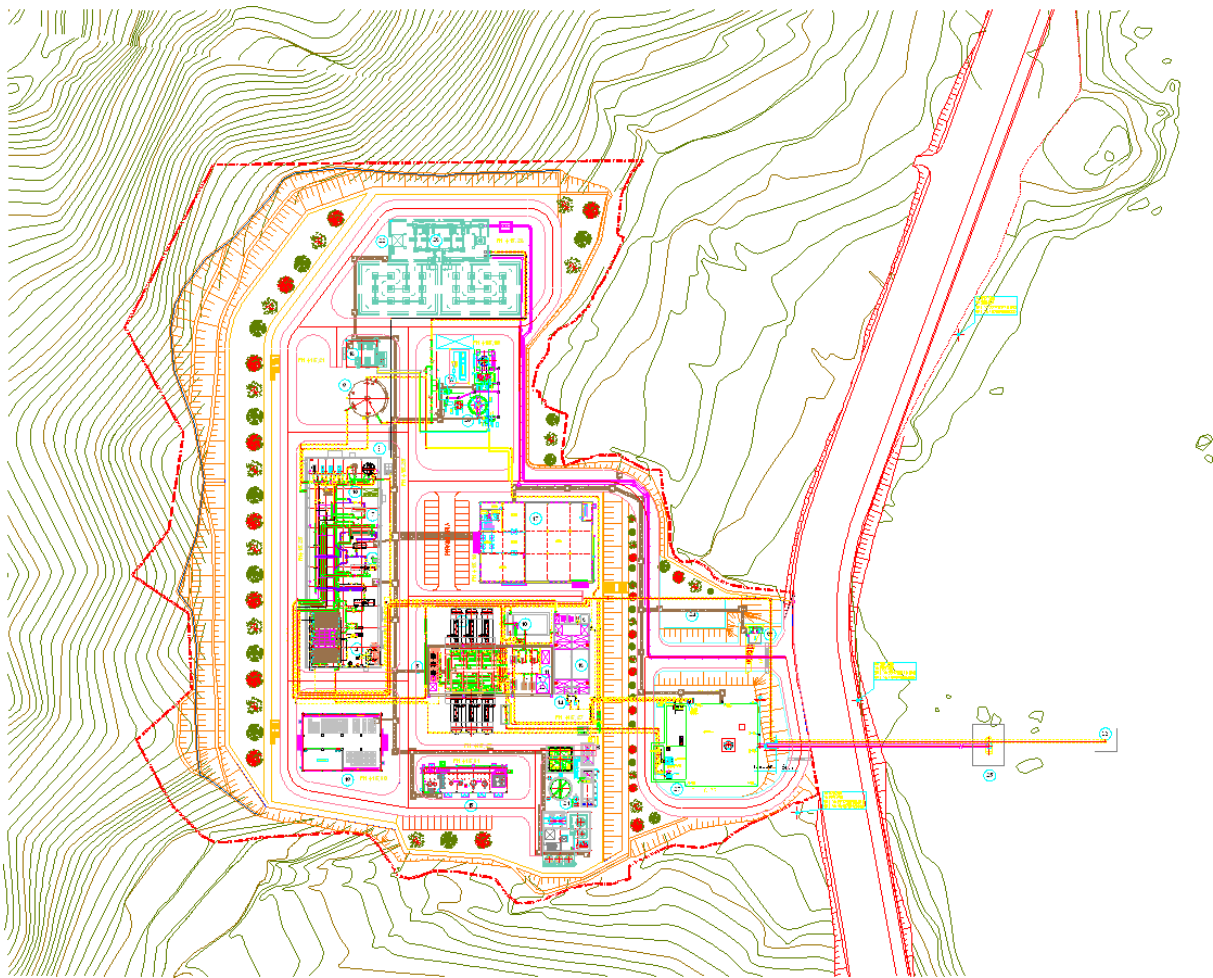
Fig. 11. Contour lines of the Gijang SWRO plant.

If the rate of flow exergies is calculated for the incoming and outgoing streams of a system, the theoretical minimum separation work of the desalination system, which separates incoming streams of saline feed water into two (one less saline product and the other more saline reject) outgoing streams, can be easily calculated:

$$W_{min,theory} = -\left(\sum \dot{E}_{in} - \sum \dot{E}_{out} \right) \tag{3}$$

Eq. (3) considers only the boundary streams of the system, thus the "theoretical" minimum separation work is not a function of internal treatment steps, which is the same philosophy
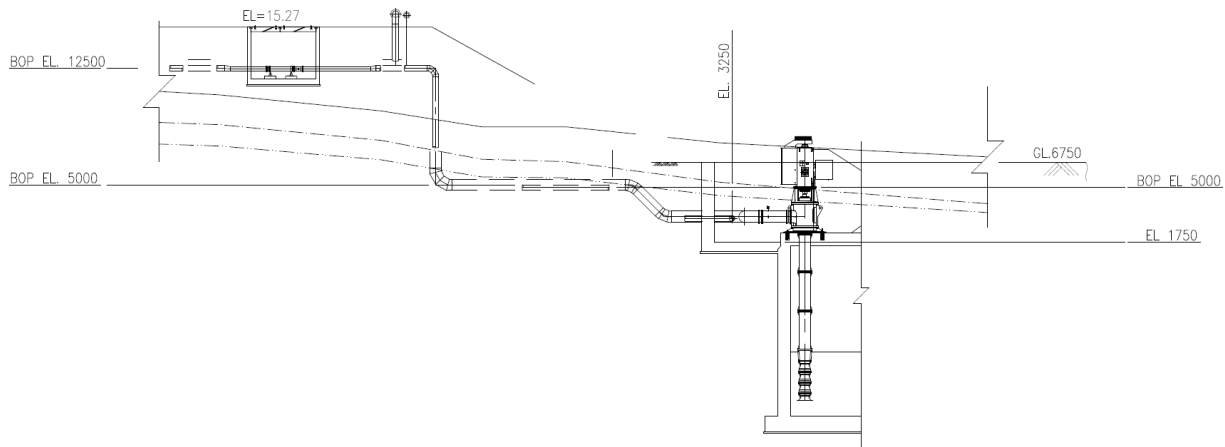
Fig. 12. Pipeline from the SSP toward pretreatment area.

to the one in the study carried out by Ihm and Woo [7]. In the meantime, the minimum work for a certain "process" shall be the sum of "exergy generation" of its "flow" exergy generating components, for example, pumps, which means the process requires that amount of energy as an input, for example, in the form of electricity, to keep the process work. Therefore,

$$W_{\text{min,process}} = -\Sigma_i \Sigma_j \dot{E}_{f,j} \quad \text{for } \forall i \text{ component where} \Sigma_j \dot{E}_{f,j} < 0 \quad (4)$$

where i stands for each component of the system including pumps, tanks, treatment steps, and so on, though the condition of Eq. (4) limits i for flow exergy generating components only. j stands for the incoming and outgoing "flow" streams for the component i.

From $W_{\text{min,process}}$, once the efficiencies of energy supply devices, for example, pumps and motors, are considered, the actual required work, W_{actual}, can be easily calculated.

$$W_{\text{actual}} = -\Sigma_i (\Sigma_j \dot{E}_{f,j} / \eta_{i,\text{device}}) \quad \text{for } \forall i \text{ component where} \Sigma_j \dot{E}_{f,j} < 0 \quad (5)$$

where $\eta_{i,\text{device}}$ is the efficiency of the energy supply device of the component i, that is, $\eta_{i,\text{device}} = $ work by the device/(electrical) energy input of the device.

Dividing $W_{\text{min,theory}}$, $W_{\text{min,process}}$, W_{actual} in (kW), by the product flow rate (ton/h) provides the specific energy consumptions $W_{\text{min,theory}}$, $W_{\text{min,process}}$, W_{actual} (kWh/ton) where W_{actual} is the specific power consumption (SPC) for a process where only electric energy is required (For a commercial/industrial desalination plant, the calculated W_{actual} is usually less than the practical SPC measured, due to the electricity consumed by auxiliary systems other than the main process pumps, which includes post treatment, wastewater treatment, chemical dosing, instruments, control valves, programmable logic controller, HVAC (heating, ventilation, and air conditioning), air conditioning, lighting and so on).

It is noted that the second law efficiency of a system can be calculated using the calculated works as follows, which are intrinsically identical to Eq. (2). The difference between Eqs. (6) and (7) comes from the difference in the system control volume whether to include a real, mechanical body of pump and motor, through which electrical energy transfers to fluids, or not. Eq. (6) describes a RO process as converting mechanical exergy into chemical exergy, while Eq. (7) describes a RO process as converting electrical energy into chemical exergy. Many prior exergy analysis studies [13,14,19] did not consider the efficiencies of pumps and motors, thus $\eta_{\text{II,process}}$ is used to evaluate a process. In the study by Sharqawy et al. [19], the exergetic efficiencies of process pumps are evaluated separately, considering pump and motor efficiencies.

$$\eta_{\text{II,process}} = W_{\text{min,theory}} / W_{\text{min,process}} = w_{\text{min,theory}} / w_{\text{min,process}} \quad (6)$$

$$\eta_{\text{II,actual}} = W_{\text{min,theory}} / W_{\text{actual}} = w_{\text{min,theory}} / w_{\text{actual}} \quad (7)$$

4.2. Evaluation of Gijang 2 MIGD line design conditions

The schematic of the Gijang 2 MIGD line is given in Fig. 13. The numbers stand for measurement points. Table 2 shows the design conditions at 25°C (summer) and at 10°C (winter). For each measurement points, the correspondent pipe diameter and the level are given for the kinetic and the potential exergy calculations. In order to have a gravitational flow from the sea to the DABF, the DABF is constructed underground, and the suction of SSP is located at the level of –3.6 m. For the SSP design head of 67 m before and 47 m after the modifications, it is noticed that 22.06 m (level difference between points 2 and 4 in Table 2) is to overcome the level difference from the suction point of SSP to the UF system. The UF filtered water tank to the SWRO system is located at the level of 16–20 m. In Table 2, it is also noticed that the feed and concentrate pressures at SWRO are the only changes at winter, while usually lower permeate total dissolved solid (TDS) should be expected due to lower seawater temperature (thus less diffusion) and a correspondent higher feed pressure at SWRO. Actually the 16 inch membrane used for this project was a proto-type and thus it was not considered in the membrane projection tool of the manufacturer, so the guaranteed TDS of 270 ppm was used for both the process flow diagrams at summer and winter.

The developed exergy function is used to evaluate the design conditions of the Gijang 2 MIGD line. At each measurement points, kinetic, potential, thermomechanical and
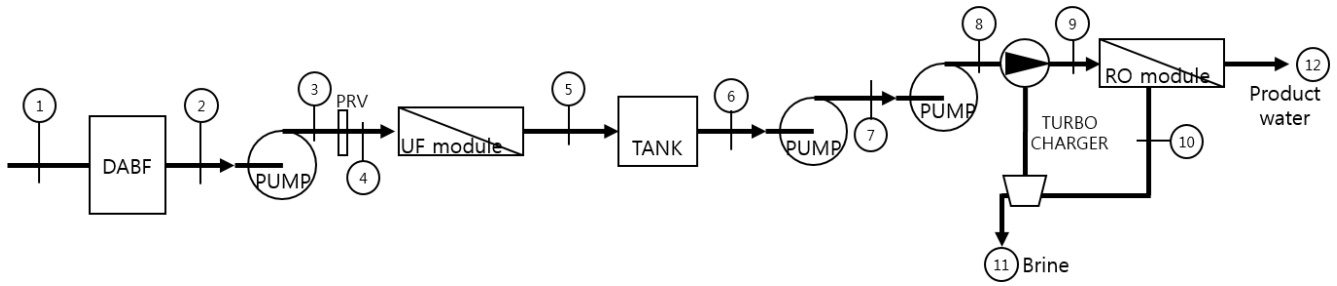
Fig. 13. Schematic of the Gijang 2 MIGD line.

Table 2
Design conditions of the Gijang 2 MIGD line

Parameter	Unit	Sea = 0	1	2	3	4	5	6	7	8	9	10	11	12
Summer condition														
Flow rate	ton/h	890	890	890	890	890	890	834	834	834	834	432	432	402
Temperature	°C	25	25	25	25	25	25	25	25	25	25	25	25	25
Pressure	barg	0	0.4	0.4	6.5	3	0.5	0	3	38.8	**55.1**	**54.1**	1.5	1
TDS	mg/L	34,458	34,458	34,458	34,458	34,458	34,458	34,458	34,458	34,458	34,458	66,444	66,444	270
Pipe diameter	mm	N/A	1200	600×3	350	350	350	350	350	350	350	350	250	200
Level	mm	0	−3,060	−3,060	3,250	19,000	16,000	16,000	16,889	16,905	19,850	17,450	16,100	16,150
Winter condition (pipe diameter and level are unchanged)														
Flow rate	ton/h	890	890	890	890	890	890	834	834	834	834	432	432	402
Temperature	°C	10	10	10	10	10	10	10	10	10	10	10	10	10
Pressure	barg	0	0.4	0.4	6.5	3	0.5	0	3	38.8	**61.8**	**59.3**	1.5	1
TDS	mg/L	34,458	34,458	34,458	34,458	34,458	34,458	34,458	34,458	34,458	34,458	66,444	66,444	270

chemical exergies are calculated as per Eq. (1), which specific exergy results are shown in Table 3. It is clear that the thermo-mechanical specific exergy at SWRO feed is higher by 11.8% at winter due to the higher required pressure of 61.8 bar instead of 55.1 bar at summer. Note that the chemical exergies at lower TDS (product water) and higher TDS (brine) compared with the reference state (seawater) becomes less at winter, by 6.4% and 8.0%, respectively, compared with the chemical exergies at summer (the same trend is found from the contours of the specific flow exergy in the study carried out by Sharqawy et al. [19]). This implies that a less theoretical minimum work would be required when the temperature is lower, while practically higher pressure is required for a membrane separation process due to less diffusivity of cooler saline water. It is also noticed that part of thermomechanical exergy (by SSP pumping pressure) at point 3 is converted to the potential exergy (from higher level) at point 4. The part of thermomechanical exergy (by HPP and T/C pumping pressure) at point 9 is converted to the chemical exergies at point 10 (higher TDS brine) and 12 (lower TDS product water) through RO membrane separation.

From the exergy balance at each component, the component-wise contribution of entropy generation is calculated and summarized in Table 4. The negative values of exergy destruction indicate that at least this amount of energy should be supplied from an external source, for example, in the form of electricity. It is noted that the energy input to the SSP should cover the sum of the negative values in the intake pipe, the DABF and the SSP. All pumps

show the similar energy consumption requirement regardless of the seasonal temperature changes, which indicates that the pumps are designed to operate at the same flow rate and at the same hydraulic head. The exergy destruction for the pumps can be easily calculated as there are the design data for power consumption, which are 288.5, 114.0 and 1,265.0 kW for the SSP, FSP and HPP, respectively. In this paper, however, the destructed exergy in the process pumps are not included in the process exergy analysis following to other researchers. Instead, the exergy destruction at pumps is considered to calculate the second law efficiency of the pumps.

From Table 4, several key design characteristics are observed. Exergy destruction mostly occurs at the SWRO membrane and the T/C, and the exergy destruction in the SWRO membrane is 56.7% more at winter probably due to the higher pressure requirement. The large amount of exergy loss in the T/C should be understood properly. The control valve at the discharge of the HPP is located "after" the pressure transmitter at the location No. 8 in Table 2 and Fig. 13. Obviously this control valve plays a key role to maintain the design pressures of 55.1 bar at summer and 61.8 bar at winter in front of the SWRO membrane, by controlling the permeate flow rate to be the same. Due to the absence of the pressure transmitter "after" this control valve, the exergy loss through the control valve and the T/C are analyzed together in the title of "T/C". Assuming the similar exergy loss through the T/C only, the difference in the exergy loss of the T/C between summer and winter, which is 94.22 kW, should be

Table 3
Exergy calculation results for the Gijang 2 MIGD line at its design conditions

No.	e_f (kJ/kg)					$\dot{E}_f$ (kJ/s)
	Kinetic	Potential	Thermomechanical	Chemical	Total	
Summer condition (25°C)						
1	0.0001	–0.0300	0.0396	0.0000	0.0097	2.39
2	0.0001	–0.0300	0.0396	0.0000	0.0097	2.40
3	0.0003	0.0319	0.6437	0.0000	0.6759	167.10
4	0.0003	0.1864	0.2971	0.0000	0.4838	119.61
5	0.0003	0.1570	0.0495	0.0000	0.2068	51.12
6	0.0003	0.1570	0.0000	0.0000	0.1572	36.43
7	0.0003	0.1657	0.2971	0.0000	0.4631	107.28
8	0.0003	0.1658	3.8425	0.0000	4.0086	928.66
9	0.0003	0.1947	**5.4567**	0.0000	5.6517	1,309.31
10	0.0001	0.1712	**5.3577**	**1.0695**	6.5984	776.85
11	0.0003	0.1579	0.1485	**1.0695**	1.3762	164.73
12	0.0006	0.1584	0.0990	**2.6046**	2.8627	319.96
Winter condition (10°C)						
1	0.0001	–0.0300	0.0395	0.0000	0.0095	2.35
2	0.0001	–0.0300	0.0395	0.0000	0.0096	2.37
3	0.0003	0.0319	0.6416	0.0000	0.6738	166.58
4	0.0003	0.1864	0.2961	0.0000	0.4828	119.37
5	0.0003	0.1570	0.0494	0.0000	0.2066	51.08
6	0.0003	0.1570	0.0000	0.0000	0.1572	36.43
7	0.0003	0.1657	0.2961	0.0000	0.4621	107.05
8	0.0003	0.1658	3.8299	0.0000	3.9960	925.74
9	0.0003	0.1947	**6.1002**	0.0000	6.2952	1,458.38
10	0.0001	0.1712	**5.8534**	**0.9834**	7.0080	824.22
11	0.0003	0.1579	0.1481	**0.9834**	1.2897	154.34
12	0.0006	0.1584	0.0987	**2.4369**	2.6947	301.20

understood as the minimum contribution from the control valve only, underlining the importance of the introduction of a VFD to the HPP.

Although the PRV is simply regulating the feed pressure to protect UF membranes, the exergy loss in the PRV, almost 66% of the exergy loss at the UF system, seems to have a surplus margin which could be optimized. It is worth to note that the theoretical minimum work at winter is 0.994 kWh/ton only while it is 1.065 kWh/ton at summer, as expected from Table 3. Finally the second law efficiency of this system is evaluated as 40.40% at summer and 37.85% at winter.

5. Results and discussion

5.1. Electrical energy consumption of the SSP

The power consumptions before and after the modifications of the SSP are compared based on the actual operation data at the Gijang SWRO plant. Fig. 14 shows the power consumption of the SSP before and after the modifications. The operational data for "before modification" are collected from 2014 to 2015, and the data for "after modification" are collected in 2016. The average power consumptions of the SSP are found to be 287 kW before the modifications and 198 kW after the modifications, thus 89 kW (31.0%) of electricity could

be saved by optimizing the pump head from 67 to 47 m by removing one of the initial four stages and by trimming the remaining impellers. Considering the water production of 402 ton/h, the modifications in the SSP contributes to reduce the SPC by 0.221 kWh/ton.

5.2. Electrical energy consumption of the HPP

Until the installation of the VFD at the end of 2015, the HPP had been operated at a constant rotating speed of 3,570 rpm, pressurizing the seawater to about 40 bar regardless of the seawater temperature. After the installation, the discharge pressure from the HPP decreases when the seawater temperature increases. Maintaining the recovery rate at the SWRO membrane about 48.4% and the fresh water production about 395–403 ton/h, the HPP with VFD automatically control its impeller rotation speed, thus optimizing the electricity consumption. Fig. 15 shows the discharge pressure of the HPP before and after the VFD installation. It is clear that the required pressure to have the same recovery and product reduces with the seawater temperature increase.

Fig. 16 shows the power consumption of the HPP before and after the VFD installation. The power consumption reduction with the increase of seawater temperature is a

Table 4
Exergetic efficiency analyses for the Gijang 2 MIGD line at its design conditions

Component	Exergy destruction		η_{II}
	(kW) ⓐ	(%) ⓐ/ⓑ	
Summer condition (25°C)			
1 Intake pipe	–2.39	N/A	N/A
2 DABF	–0.01	N/A	100.47%
3 SSP	–164.70	N/A	57.92%
4 PRV	47.49	7.5%	71.58%
5 UF	71.70	11.4%	41.62%
6 Tank	11.48	1.8%	77.55%
7 FSP	–70.85	N/A	71.31%
8 HPP	–821.38	N/A	67.67%
9 T/C	231.46	36.7%	86.43%
10 SWRO membrane	212.51	33.7%	83.77%
11 Product line	11.42	1.8%	96.43%
12 Discharge line	45.31	7.2%	72.50%
SUM (1–12) (kW)	631.36	N/A	N/A
SUM (4–6, 9–12) (kW) ⓑ	427.96	100.0%	N/A
$W_{min,theory}$ from Eq. (3) (kW)	427.96 (w = 1.065 kWh/ton)		100.00%
$W_{min,process}$ from Eq. (4) (kW)	1,059.33 (w = 2.635 kWh/ton)		40.40%
W_{actual} from Eq. (5) (kW)	1,667.50 (w = 4.148 kWh/ton)		25.66%
Winter condition (10°C)			
1 Intake pipe	–2.35	N/A	N/A
2 DABF	–0.01	N/A	100.47%
3 SSP	–164.21	N/A	57.74%
4 PRV	47.21	7.2%	71.66%
5 UF	71.50	10.9%	41.67%
6 Tank	11.44	1.7%	77.60%
7 FSP	–70.62	N/A	71.16%
8 HPP	–818.69	N/A	67.47%
9 T/C	137.24	20.9%	92.16%
10 SWRO membrane	332.96	50.7%	77.17%
11 Product line	11.39	1.7%	96.22%
12 Discharge line	44.52	6.8%	71.15%
SUM (1–12) (kW)	656.26	N/A	N/A
SUM (4–6, 9–12) (kW) ⓑ	399.62	100.0%	N/A
$W_{min,theory}$ from Eq. (3) (kW)	399.62 (w = 0.994 kWh/ton)		100.00%
$W_{min,process}$ from Eq. (4) (kW)	1,055.89 (w = 2.627 kWh/ton)		37.85%
W_{actual} from Eq. (5) (kW)	1,667.50 (w = 4.148 kWh/ton)		23.97%

well-known benefit from VFD. Before the VFD, the HPP was operated at a fixed constant speed and it consumed about 1,260–1,290 kW. With the VFD, the power consumption of the HPP is lowered, in the range of 964–1,155 kW. Therefore, 105–326 kW of electricity is saved from the introduction of VFD to the HPP. Considering the water production of 402 ton/h, this is 0.261–0.811 kWh/ton reduction in terms of SPC.

5.3. Second law efficiency evaluation

The pump modification works are evaluated by analyzing the operation data in terms of exergetic efficiency. Two daily averaged data are carefully selected, one before and the other after the modification works, which are given in Table 5. A similar daily averaged seawater temperature is considered for a pair comparison during the selection. As can be seen, the discharge pressure of the SSP is reduced from 5.8 to 4.35 bar while the UF feed pressure remains similar. The discharge pressure of the HPP is also reduced from 40.0 to 36.46 bar while the SWRO feed pressure remains similar. Therefore, it is easily concluded that the pump modification works are completed successfully and the unnecessary pressure drops at the PRV after the SSP and at the control valve after the HPP are optimized.

Tables 6 and 7 summarize the exergy analysis results. There are specific thermomechanical exergy drops after the SSP (at point 3) and the HPP (at point 8) due to less pressure requirement. From Table 7, it is very clear that the required exergy for the modified pumps are due to the less exergy

destruction at the following valves. The required energy input to the SSP is reduced by 37.15 kW when the exergy loss at the PRV is reduced by 36.75 kW. Similarly, the required energy input to the HPP is reduced by 78.58 kW when the exergy loss at the T/C is reduced by 89.29 kW. Finally the second law efficiency of the overall process is enhanced from 42.83% to 46.61%, and the SPC is reduced from 4.213 to 3.493 kWh/ton for this Gijang 2 MIGD line based on the first pass permeate flow rate.

6. Conclusion

As a Korean government R&D program, efforts to enhance the Gijang SWRO desalination plant in Busan, Korea, is on-going. The design conditions of the SSP and the HPP, the two major components in terms of electrical energy consumption, are carefully reviewed for optimization with considerations of a stable operation at their practical operation range. The hydraulic head of the SSP is decided to reduce from its original 67 m to 47 m by impeller redesign. A VFD is installed to the HPP for the optimal operation depending on the required feed pressure at the SWRO membrane, which varies on the seawater temperature. The operation data of before-modification (2014–2015) and after-modification (2016) confirm the electrical energy saving of average 89 kW from the SPP modification and
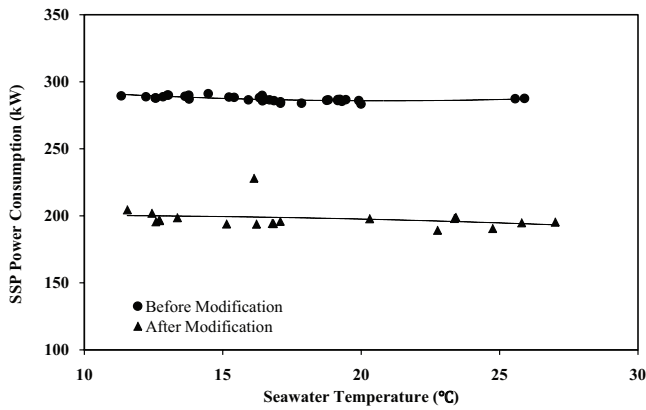
Fig. 14. Power consumption of the SSP before and after the modifications.
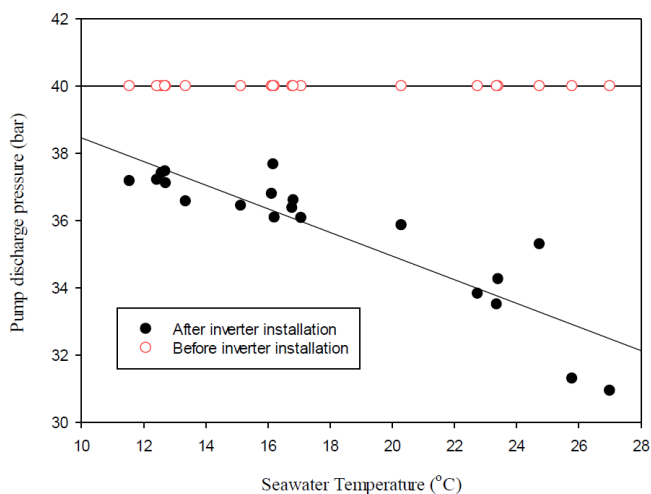
Fig. 15. Discharge pressure of the HPP before and after the inverter (VFD) installation.
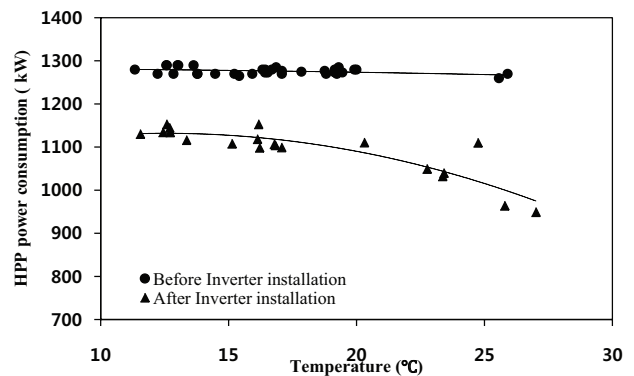
Fig. 16. Power consumption of the HPP before and after the inverter (VFD) installation.

Table 5
Daily averaged operation data before and after the pump modifications

Parameter	Unit	Sea = 0	1	2	3	4	5	6	7	8	9	10	11	12
Before – June 17, 2015														
Flow rate	ton/h	919.34	919.34	913.96	913.96	911.24	911.24	829.49	829.49	829.49	829.49	434.01	434.01	395.48
Temperature	°C	15.46	15.46	15.46	15.46	15.46	15.46	15.46	15.46	15.46	15.46	15.46	15.46	15.46
Pressure	barg	0	0.4	0.4	5.8	1.5	1.25	0	1.38	**40**	**54.11**	53.44	1.5	1.77
TDS	mg/L	35,808	35,808	35,808	35,808	35,808	35,808	35,808	35,808	35,808	35,808	73,199	73,199	327
After – May 31, 2016														
Flow rate	ton/h	912.39	912.39	907.91	907.91	909.61	909.61	831.95	831.95	831.95	831.95	428	428	403.95
Temperature	°C	16.2	16.2	16.2	16.2	16.2	16.2	16.2	16.2	16.2	16.2	16.2	16.2	16.2
Pressure	barg	0	0.4	0.4	4.35	1.49	1.23	0	1.38	**36.46**	**54.14**	53.45	1.5	1.78
TDS	mg/L	36,732	36,732	36,732	36,732	36,732	36,732	36,732	36,732	36,732	36,732	70,875	70,875	556

Table 6
Exergy calculation results from the operation data before and after the pump modifications

No.	e_f (kJ/kg)					$\dot{E}_f$ (kJ/s)
	Kinetic	Potential	Thermomechanical	Chemical	Total	
Before – June 17, 2015						
1	0.0001	–0.0300	0.0395	0.0000	0.0095	2.43
2	0.0001	–0.0300	0.0395	0.0000	0.0096	2.43
3	0.0003	0.0319	**0.5725**	0.0000	0.6047	153.52
4	0.0003	0.1864	0.1481	0.0000	0.3348	84.74
5	0.0003	0.1570	0.1234	0.0000	0.2807	71.04
6	0.0003	0.1570	0.0000	0.0000	0.1572	36.23
7	0.0003	0.1657	0.1362	0.0000	0.3022	69.62
8	0.0003	0.1658	**3.9481**	0.0000	4.1142	947.97
9	0.0003	0.1947	**5.3408**	0.0000	5.5358	1,275.52
10	0.0001	0.1712	5.2747	1.2497	6.6956	789.75
11	0.0003	0.1579	0.1481	1.2497	1.5560	187.09
12	0.0006	0.1584	0.1747	2.6229	2.9567	325.33
After – May 31, 2016						
1	0.0001	–0.0300	0.0395	0.0000	0.0095	2.41
2	0.0001	–0.0300	0.0395	0.0000	0.0095	2.41
3	0.0003	0.0319	**0.4291**	0.0000	0.4613	116.35
4	0.0003	0.1864	0.1470	0.0000	0.3337	84.32
5	0.0003	0.1570	0.1213	0.0000	0.2786	70.40
6	0.0003	0.1570	0.0000	0.0000	0.1572	36.34
7	0.0003	0.1657	0.1361	0.0000	0.3021	69.81
8	0.0003	0.1658	**3.5967**	0.0000	3.7628	869.58
9	0.0003	0.1947	**5.3408**	0.0000	5.5358	1,279.32
10	0.0001	0.1712	5.2728	1.0436	6.4876	755.58
11	0.0003	0.1579	0.1480	1.0436	1.3498	160.03
12	0.0006	0.1584	0.1756	2.6801	3.0148	338.83

105–326 kW from the introduction of VFD to the HPP. These amounts count for 0.221 and 0.261–0.811 kWh/ton reduction in the SPC.

Exergy analyses are conducted to examine the operation data before and after the modifications. At a similar seawater temperature of about 16°C, it is found that the second law efficiency is improved from 42.83% to 46.61% with the SPC drop from 4.213 to 3.493 kWh/ton based on the first pass SWRO permeate flow rate. The exergy destruction comparison shows that these benefits are caused from the minimized exergy loss at the PRV after the SSP and at the control valve after the HPP after the pump modifications.

From the comparison of electricity consumption and the second law analyses from the actual plant operation data, the energy efficiency improvement of the Gijang 2 MIGD line has been confirmed and the pump impeller redesign and the introduction of VFD are found to be very useful and practical methods. Because exergy analyses provide component-wise efficiencies, a real-time evaluation system, which would show the trend graph of efficiencies of each component as well as the overall process from the real-time plant operation data, could be considered in a near future for efficient operation and maintenance.

Symbols

DABF	—	Dissolved air flotation with ball filter
FSP	—	Filtered water supply pump
HPP	—	High pressure pump
HVAC	—	Heating, ventilation and air conditioning
MED	—	Multi-effect distillation
MIGD	—	Million imperial gallons per day (1 MIGD = 4,546 m³/d water production)
MVC	—	Mechanical vapor compressor
PRO	—	Pressure retarded osmosis
PRV	—	Pressure regulating valve
RO	—	Reverse osmosis
SPC	—	Specific power consumption
SSP	—	Seawater supply pump
SWRO	—	Seawater reverse osmosis
TDS	—	Total dissolved solids
TVC	—	Thermo vapor compressor
T/C	—	Turbocharger
UF	—	Ultrafiltration
VFD	—	Variable frequency drive
$\dot{E}$	—	Exergy rate, kJ/s
e	—	Specific exergy, kJ/kg
g	—	Gravitational acceleration, 9.81 m/s²
h	—	Specific enthalpy, kJ/kg

Table 7
Exergetic efficiency analyses from the operation data before and after the pump modifications

Component	Exergy destruction		η_{II}
	(kW) ⓐ	(%) ⓐ/ⓑ	
Before June 17, 2015			
1 Intake pipe	–2.43	N/A	N/A
2 DABF	0.00	N/A	99.90%
3 SSP	**–151.09**	N/A	53.49%
4 PRV	**68.78**	11.3%	55.20%
5 UF	20.08	3.3%	77.96%
6 Tank	28.43	4.7%	59.99%
7 FSP	–33.39	N/A	46.34%
8 HPP	**–878.35**	N/A	71.03%
9 T/C	**275.11**	45.2%	84.17%
10 SWRO membrane	160.44	26.3%	87.42%
11 Product line	19.79	3.2%	93.92%
12 Discharge line	36.43	6.0%	80.53%
SUM (1–12) (kW)	456.21	N/A	N/A
SUM (4–6, 9–12) (kW) ⓑ	609.05	100.0%	N/A
$W_{min,theory}$ from Eq. (3) (kW)	456.2 (w = 1.154 kWh/ton)		100.00%
$W_{min,process}$ from Eq. (4) (kW)	1,065.3 (w = 2.694 kWh/ton)		42.83%
W_{actual} from Eq. (5) (kW)	1,666.0 (w = 4.213 kWh/ton)		27.38%
After May 31, 2016			
1 Intake pipe	–2.41	N/A	N/A
2 DABF	0.00	N/A	99.99%
3 SSP	**–113.94**	N/A	58.76%
4 PRV	**32.03**	6.3%	72.47%
5 UF	19.94	3.9%	77.93%
6 Tank	28.04	5.5%	60.17%
7 FSP	–33.48	N/A	46.44%
8 HPP	**–799.77**	N/A	74.40%
9 T/C	**185.82**	36.6%	88.57%
10 SWRO membrane	184.90	36.5%	85.55%
11 Product line	20.33	4.0%	94.00%
12 Discharge line	35.96	7.1%	77.53%
SUM (1–12) (kW)	442.58	N/A	N/A
SUM (4–6, 9–12) (kW) ⓑ	507.02	100.0%	N/A
$W_{min,theory}$ from Eq. (3) (kW)	442.6 (w = 1.096 kWh/ton)		100.00%
$W_{min,process}$ from Eq. (4) (kW)	949.6 (w = 2.351 kWh/ton)		46.61%
W_{actual} from Eq. (5) (kW)	1,411.0 (w = 3.493 kWh/ton)		31.34%

l	—	Level, mm, m
P	—	Pressure, Pa, bar
s	—	Specific entropy, kJ/kgK
T	—	Temperature, K
V	—	Volume, m³
v	—	Velocity, m/s
W	—	Work, kJ, kWh
w	—	Specific work, kJ/kg, kWh/ton
X	—	Salinity, g/kg, %, ppm
y	—	mass fraction
η	—	Efficiency
μ_i	—	Chemical potential of the i-th component, kJ/mol
σ	—	Standard deviation

References

[1] Available at: http://edition.cnn.com/2017/07/21/asia/north-korea-drought/index.html (Accessed 5 September 2017).
[2] Available at: http://www.koreatimes.co.kr/www/nation/2017/06/371_231587.html (Accessed 5 September 2017).
[3] S.W. Woo, B.S. Park, W.N. Lee, Y.H. Park, J.H. Min, S.W. Park, S.N. You, G.J. Jun, Y.J. Baek, Seawater intake system in Test Bed

seawater reverse osmosis (SWRO) project, Desal. Wat. Treat., 51 (2013) 6238–6247.

[4] W.N. Lee, S.W. Woo, B.S. Park, J.J. Lee, J.H. Min, S.W. Park, S.N. You, G.J. Jun. Y.J. Baek, Economic feasibility study for MF system as a pretreatment of SWRO in test bed desalination plant, Desal. Wat. Treat., 51 (2013) 6248–6258.

[5] W. Lee, C.O. Kwon, G. Jun, B. Park, J. Lee, J. Min, S. Park, S. You, S. Woo, Design and Commissioning of Busan Gijang SWRO Desalination Plant Using 16-inch Membranes in Korea, IDA World Congress on Desalination and Water Reuse, IDAWC 51480, August 30–September 4, San Diego, CA, USA, 2015.

[6] WATEREUSE Association Desalination Committee, Seawater Desalination Costs, White Paper, 2012.

[7] S. Ihm, S. Woo, Comparative study on the methods of calculating theoretical minimum energy requirement for desalination, Desal. Wat. Treat., 90 (2017) 32–45.

[8] WATEREUSE Association Desalination Committee, Seawater Desalination Power Consumption, White Paper, 2011.

[9] S. Shiels, When trimming a centrifugal pump impeller can save energy and increase flow rate, World Pumps, 1999 (1999) 37–40.

[10] P. Zhou, J. Tang, J. Mou, B. Zhu, Effect of impeller trimming on performance, World Pumps, 2016 (2016) 38–41.

[11] R. Camoirano, G. Dellepiane, Variable frequency drives for MSF desalination plant and associated pumping stations, Desalination, 182 (2005) 53–65.

[12] S. Prachyl, Variable Frequency Drives and Energy Savings, White Paper, Siemens, 2010.

[13] O.A. Hamed, A.M. Zamamiri, S. Aly, N. Lior, Thermal performance and exergy analysis of a thermal vapor compression desalination, Energy Convers. Manage., 37 (1996) 379–387.

[14] K.H. Mistry, R.K. McGovern, G.P. Thiel, E.K. Summers, S.M. Zubair, J.H. Lienhard V, Entropy generation analysis of desalination technologies, Entropy, 13 (2011) 1829–1864.

[15] A.M. Blanco-Marigorta, A. Lozano-Medina, J.D. Marcos, The exergetic efficiency as a performance evaluation tool in reverse osmosis desalination plants in operation, Desalination, 413 (2017) 19–28.

[16] Available at: www.khoa.go.kr (Accessed 22 September 2017).

[17] V. Tutterow, G. Hovstadius, A. McKane, Going with the Flow: Life Cycle Costing for Industrial Pumping Systems. Available at: https://www.osti.gov/scitech/servlets/purl/894551-EXEiEl/ (Accessed 11 January 2018).

[18] Available at: https://www.ksb.com/centrifugal-pump-lexicon/impeller-trimming/192440/ (Accessed 22 September 2017).

[19] M.H. Sharqawy, J.H. Lienhard V, S.M. Zubair, Second law analysis of reverse osmosis desalination plants: an alternative design using pressure retarded osmosis, Energy, 36 (2011) 6617–6626.

[20] T. Gundersen, An Introduction to the Concept of Exergy and Energy Quality, Department of Energy and Process Engineering, Norwegian University of Science and Technology, Trondheim, Norway, Vol. 3, 2009.

[21] A. Ghannadzadeh, Exergetic Balances and Analysis in a Process Simulator: A Way to Enhance Process Energy Integration, Ph.D. Thesis, University of Toulouse, 2012.

[22] M.H. Sharqawy, J.H. Lienhard V, S.M. Zubair, Thermophysical properties of seawater: a review of existing correlations and data, Desal. Wat. Treat., 16 (2010) 354–380.

[23] Y. Cerci, Exergy analysis of a reverse osmosis desalination plant in California, Desalination, 134 (2002) 257–266.

Appendix A. Validation of flow exergy function

The excel-based flow exergy function is developed based on a study by Sharqawy et al. [19]. In this Appendix, only the thermomechanical and the chemical components of exergy is of interest for validation purpose, thus the following equation is considered instead of Eq. (1).

$$e_f = \left(h - h^*\right) - T_0\left(s - s^*\right) + \sum_{i=1}^{n} y_i\left(\mu_i^* - \mu_i^0\right) \tag{A1}$$

A.1. Exemplary calculation

In order to validate the developed exergy function, the same examples are considered in the study by Sharqawy et al. [19]. For the calculation of specific flow exergy of the seawater at $T = 50°C$, $X_s = 50$ g/kg and $P = 103.325$ kPa, the environment conditions are selected as $T_0 = 25°C$, $X_{s,0} = 35$ g/kg and $P_0 = 103.325$ kPa. In Table A1, the calculation results for each specific quantities and the resultant specific flow exergy are compared with the calculation results of the study by Sharqawy et al. [19]. The same property equations of the study by Sharqawy et al. [22] are used.

It is noted that the most of the calculation difference comes from the use of 0°C = 273.15 K in this paper instead of 0°C = 273 K in the study by Sharqawy et al. [19]. The following example shows 1.15% difference in the flow exergy calculations due to the use of 273.15 K instead of 273 K.

$e_f = (195.860 \quad - \quad 97.484) \quad - \quad 298 \quad \times \quad (0.6543 \quad - \quad 0.3373)$
$\quad\quad + 0.05 \times (103.304 - 70.866) + 0.95 \times (-8.691 + 7.276)$
$\quad\quad = 4.188$ kJ/kg

$e_f = (195.860 \quad - \quad 97.484) \quad - \quad 298.15 \quad \times \quad (0.6545 \quad - \quad 0.3373)$
$\quad\quad + 0.05 \times (103.304 - 70.866) + 0.95 \times (-8.691 + 7.276)$
$\quad\quad = 4.140$ kJ/kg

Table A1
Comparison of calculation results for specific properties and flow exergy ($T = 50$ °C, $X_s = 50$ g/kg, $P = 103.325$ kPa and $T_0 = 25$ °C, $X_{s,0} = 35$ g/kg, $P_0 = 103.325$ kPa)

Calculation	Ref. [19] (A)	Present work (B)	% Deviation (B/A-1)
h (kJ/kg)	195.860	195.860	0.00%
h^* (kJ/kg)	97.484	97.484	0.00%
s (kJ/kgK)	0.6543	0.6543	0.01%
s^* (kJ/kgK)	0.3373	0.3373	0.01%
μ_w^* (kJ/kg)	−8.691	−8.693	0.02%
μ_w^0 (kJ/kg)	−7.276	−7.279	0.03%
μ_s^* (kJ/kg)	103.304	103.246	−0.06%
μ_s^0 (kJ/kg)	70.866	70.814	−0.07%
e_f (kJ/kg)	4.188	4.143	−1.07%

The remaining difference comes from the significant number – limited significant number is used in the study by Sharqawy et al. [19] probably to show the calculation steps one by one.

Then, the specific flow exergies are calculated for the range of 10°C–90°C in temperature and 0–100 g/kg in salinity. The contour lines are compared in Fig. A1, which shows a good agreement with the study by Sharqawy et al. [19]. From Fig. A1, it is important to understand that the separation of given saline water at reference salinity into less saline water (product) and more saline water (rejected brine) requires exergy input, which may need to be equal to or higher than the theoretical minimum work at the given salinity and temperature.

A.2. RO and RO-PRO cases

As a practical example, the BWRO case of a study carried out by Cerci [23] is employed, and the results are compared with source study [23] and the study carried out by Sharqawy et al. [19]. The configuration details can be found either in the study by Cerci [23] or in the study by Sharqawy et al. [19]. Only the key results are presented here for a validation purpose through Tables A2 and A3. The calculated thermodynamic properties and exergy analysis results show a good agreement with the study by Sharqawy et al. [19].

Another practical example is the modified case of the above, which integrates pressure retarded osmosis (PRO) as described in the study by Sharqawy et al. [19]. It seems the flow
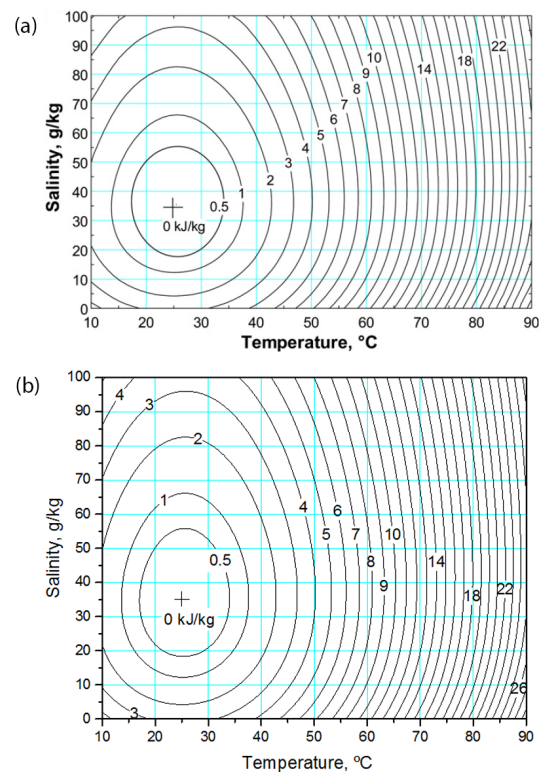

Fig. A1. Specific flow exergy contours at $P = P_0 = 101.325$ kPa, $T_0 = 25°C$, $X_{s,0} = 35$ g/kg ((a): [19], (b): reproduction in this paper).

Table A2
Thermodynamic properties at various locations for the BWRO plant

No.	P, bar	T, °C	w_s, g/kg	$\dot{m}$, kg/s	e_f kJ/kg			% Deviation (B/A-1)
					Ref. [23]	Ref. [19] (A)	Present work (B)	
0	1.013	15.0	1.55	112.65	0.0000	0.0000	0.0000	0.00%
1	3.840	15.0	1.55	112.65	0.2824	0.2827	0.2864	1.32%
2	3.840	15.0	1.55	100.66	0.2824	0.2827	0.2864	1.32%
3	3.840	15.0	1.55	11.99	0.2824	0.2827	0.2864	1.32%
4	1.013	15.0	1.55	11.99	0.0000	0.0000	0.0000	0.00%
5	3.702	15.0	1.55	100.66	0.2686	0.2689	0.2724	1.32%
6	3.564	15.0	1.55	100.66	0.2548	0.2551	0.2585	1.32%
7	16.871	15.0	1.55	100.66	1.5841	1.5860	1.6067	1.30%
8	1.013	15.0	0.02	75.37	0.5376	0.0090	0.0090	−0.23%
9	12.251	15.0	6.11	25.29	−0.1477	1.1960	1.2105	1.21%
10	6.529	15.0	6.11	25.29	−0.7185	0.6255	0.6328	1.17%
11	3.905	15.0	6.11	25.29	−0.9803	0.3640	0.3679	1.07%
12	1.013	15.0	6.11	25.29	−1.2688	0.0759	0.0759	0.01%
13	1.013	15.0	0.23	87.36	0.4489	0.0067	0.0067	−0.42%
14	1.013	15.0	0.23	87.36	0.4489	0.0067	0.0067	−0.42%

Table A3
Exergy analysis results for the BWRO plant

Exergy destroyed/input, kW	Ref. [23]	Ref. [19] (A)	Present work (B)	% Deviation (B/A-1)
Low pressure pump ⓑ	−31.81	−31.85	−32.27	1.32%
Throttling valve 1	3.39	3.39	3.43	1.32%
Static mixer	1.39	1.39	1.41	1.32%
Cartridge filter	1.39	1.39	1.41	1.32%
Main pump ⓒ	−133.81	−133.97	−135.71	1.30%
RO membrane	122.67	128.72	130.44	1.33%
Throttling valve 2	14.44	14.43	14.61	1.26%
Throttling valve 3	6.62	6.61	6.70	1.31%
Brine discharge	7.30	7.29	7.38	1.34%
Mixing chamber	1.30	0.09	0.09	0.93%
Degasifier	0.00	0.00	0.00	0.00%
Minimum separation work ⓐ, kW	7.13	2.50	2.50	-0.09%
Second law efficiency = - ⓐ/(ⓑ+ⓒ)	4.30%	1.51%	1.49%	−1.37%

rates at locations No. 7, 8 and 15 are not correct in the study by Sharqawy et al. [19], which can be easily revised from the salt and mass balances at No. 7 with No. 5 and 15. The calculation results are presented through Tables A4 and A5. The study by Sharqawy et al. [19] did not show component-wise exergy analysis (Table A5) and claimed about 21% of the second law efficiency of the BWRO-PRO system with the water permeability A = 7.9 kg/s kPa. Present reproduction estimates 20.58% of the second law efficiency in terms of process efficiency (i.e., the efficiencies of process pumps and PRO hydro-pumps are not considered), thus it could be concluded that the flow exergy function in this study is validated for this case as well.

However, it should be noted that this high second law efficiency is practically not achievable for this BWRO-PRO case. As seen in Table A4, the salinity at No. 11 is 0.293 g/kg while it should be larger than 1.55 g/kg and the salinity at No. 12 is

7.75 g/kg while it should be less than 6.11 g/kg, considering natural diffusion phenomenon in PRO – pure water shall flow from lower concentration to higher concentration only, trying to make a balance in concentration. This is the reason that the exergy is "generated" (negative value of exergy destruction) at the PRO membrane in Table A5 and therefore the PRO part at this condition is meaningless from the fact that the generated exergy through PRO hydro-turbines 1 and 2 barely a bit exceeds the required energy for the PRO pump and the PRO membrane. In order to make the considered PRO to be physically valid, the new salt and mass balances are studied and the results are given in Tables A6 and A7. Though the calculated case is at the ideal limiting condition of no exergy destruction at the PRO membrane, the second law efficiency of this BWRO-PRO system is calculated as 0.50% which is even smaller than 1.49% of the BWRO only system.

Table A4
Thermodynamic properties at various locations for the BWRO-PRO plant

No.	P, bar	T, °C	w_s, g/kg	$\dot{m}$, kg/s	e_f kJ/kg		% Deviation (B/A-1)
					Ref. [19] (A)	Present work (B)	
0	1.013	15.0	1.550	100.66	0.0000	0.0000	0.00%
1	3.840	15.0	1.550	100.66	0.2825	0.2864	1.39%
2	3.702	15.0	1.550	100.66	0.2687	0.2724	1.39%
3	3.564	15.0	1.550	100.66	0.2550	0.2585	1.36%
4	16.870	15.0	1.550	100.66	1.5849	1.6066	1.37%
5	1.013	15.0	0.020	75.37	0.0090	0.0090	−0.23%
6	12.250	15.0	6.110	25.29	1.1957	1.2104	1.23%
7	1.013	15.0	0.230	325.21	0.0067	0.0067	−0.38%
8	1.013	15.0	0.230	325.21	0.0067	0.0067	−0.42%
9	1.013	15.0	1.550	627.90	0.0000	0.0000	0.00%
10	11.610	15.0	1.550	627.90	1.0599	1.0736	1.30%
11	12.250	15.0	0.293	527.60	1.1310	1.1456	1.29%
12	11.610	15.0	7.750	125.60	1.1935	1.2070	1.13%
13	1.013	15.0	0.293	527.60	0.0060	0.0060	0.79%
14	1.013	15.0	0.293	277.76	0.0060	0.0060	0.79%
15	1.013	15.0	0.293	249.84	0.0060	0.0060	0.79%
16	1.013	15.0	7.750	125.60	0.1385	0.1385	−0.02%

Table A5
Exergy analysis results for the BWRO-PRO plant

Exergy destroyed/input, kW	Estimated from Ref. [19] (A)	Present work (B)	% Deviation (B/A-1)
Low pressure pump ⓑ	−28.44	−28.83	1.39%
Static mixer	1.39	1.41	1.32%
Cartridge filter	1.38	1.41	2.05%
Main pump ⓒ	−133.87	−135.70	1.37%
RO membrane	128.62	130.43	1.41%
Mixing chamber	0.00	0.02	−1,199%
Degasifier	0.00	0.00	0.00%
PRO pump ⓓ	−665.51	−674.14	1.30%
PRO membrane	−50.87	−51.29	0.82%
PRO turbine 1 ⓔ	132.51	134.20	1.28%
PRO turbine 2 ⓕ	593.55	601.25	1.30%
Discharge	0.00	0.00	0.00%
Minimum separation work ⓐ, kW	21.24	21.24	0.00%
Second law efficiency = − ⓐ/(ⓑ+ⓒ+ⓓ+ⓔ+ⓕ)	20.87%	20.58%	−1.41%

Table A6
Thermodynamic properties at various locations for the BWRO-PRO plant – revised calculation

No.	*P*, bar	*T*, °C	w_s, g/kg	ṁ, kg/s	e_f, kJ/kg
0	1.013	15.0	1.550	100.66	0.0000
1	3.840	15.0	1.550	100.66	0.2864
2	3.702	15.0	1.550	100.66	0.2724
3	3.564	15.0	1.550	100.66	0.2585
4	16.870	15.0	1.550	100.66	1.6066
5	1.013	15.0	0.020	75.37	0.0090
6	12.250	15.0	6.110	25.29	1.2104
7	1.013	15.0	0.230	87.36	0.0067
8	1.013	15.0	0.230	87.36	0.0067
9	1.013	15.0	1.550	627.90	0.0000
10	11.610	15.0	1.550	627.90	1.0736
11	12.205	15.0	1.550	99.69	1.1339
12	11.565	15.0	1.758	553.50	1.0690
13	1.013	15.0	1.550	99.69	0.0000
14	1.013	15.0	1.550	87.70	0.0000
15	1.013	15.0	1.550	11.99	0.0000
16	1.013	15.0	1.758	553.50	0.0002

Table A7
Exergy analysis results for the BWRO-PRO plant – revised calculation

Exergy destroyed/input, kW	Present work
Low pressure pump ⓑ	−28.83
Static mixer	1.41
Cartridge filter	1.41
Main pump ⓒ	−135.70
RO membrane	130.43
Mixing chamber	0.09
Degasifier	0.00
PRO pump ⓓ	−674.14
PRO membrane	0.00
PRO turbine 1 ⓔ	591.62
PRO turbine 2 ⓕ	113.04
Discharge	0.00
Minimum separation work ⓐ, kW	0.67
Second law efficiency = − ⓐ/(ⓑ+ⓒ+ⓓ+ⓔ+ⓕ)	0.50%